Tropical Atlantic Dust and Smoke Aerosol Variabilities related to the Madden-Julian Oscillation in MODIS and MISR Observations

Yanjuan Guo[1, 2], Baijun Tian[1], Ralph A. Kahn[3], Olga Kalashnikova[1], Sun Wong[1], and Duane E. Waliser[1]

[1]*Jet Propulsion Laboratory, California Institute of Technology, Pasadena, CA*

2. Joint Institute for Regional Earth System Science & Engineering, University of California, Los Angeles, CA

[3]*NASA Goddard Space Flight Center, Greenbelt, MD*

J. Geophys. Res – Atmosphere

To be submitted, 04/04/2012

Corresponding author address: Baijun Tian, Jet Propulsion Laboratory, M/S 233-304, California Institute of Technology, 4800 Oak Grove Dr., Pasadena, CA 91109. E-mail: baijun.tian@jpl.nasa.gov

Abstract

In this study, MODIS fine mode fraction and MISR non-spherical fraction are used to derive dust and smoke AOT components (τ_{dust} and τ_{smoke}) over the tropical Atlantic, and their variabilities related to the Madden-Julian Oscillation (MJO) are then investigated.

Both MODIS and MISR show a very similar dust and smoke winter climatology. τ_{dust} is found to be the dominant aerosol component over the tropical Atlantic while τ_{smoke} is significantly smaller than τ_{dust}. The daily MODIS and MISR τ_{dust} are overall highly correlated, with the correlation coefficients typically about 0.7 over the North Atlantic. The consistency between the MODIS and MISR dust and smoke aerosol climatology and daily variations give us confidence to use these two data sets to investigate their relative contributions to the total AOT variation associated with the MJO. However, unlike the MISR dust discrimination, which is based on particle shape retrievals, the smoke discrimination is less certain, based on assumed partitioning of maritime aerosol for both MISR and MODIS.

The temporal evolution and spatial patterns of the τ_{dust} anomalies associated with the MJO are consistent between MODIS and MISR. The τ_{dust} anomalies are very similar to those of τ anomalies, and are of comparable magnitude. In contrast, the MJO-related τ_{smoke} anomalies are rather small, and the τ_{mar} anomalies are negligible. The consistency between the MODIS and MISR results suggests that dust aerosol is the dominant component on the intra-seasonal time scale over the tropical Atlantic Ocean.

1. Introduction

The Madden-Julian Oscillation (MJO) [*Madden and Julian*, 1971; 1972] is the dominant form of the intra-seasonal (30–90 day) variability in the tropical atmosphere. It is characterized by slow (~5 m s^{-1}) eastward-propagating, large-scale oscillations in the tropical deep convection over the equatorial Indian Ocean and western Pacific during boreal winter (November–April) [*Lau and Waliser*, 2005; *Zhang*, 2005]. Recently, there is an emerging strong interest in the impacts of the MJO on atmospheric composition [*Tian and Waliser*, 2011], such as aerosol [*Tian et al.*, 2008; 2011], ozone [*Tian et al.*, 2007; *Weare*, 2010; *Li et al.*, 2011], carbon dioxide [*Li et al.*, 2010], and carbon monoxide [*Wong and Dessler*, 2007].

Tian et al. [2008] first examined the aerosol variability related to the MJO using global aerosol products from multiple sensors on various satellite platforms. That study revealed large intra-seasonal variations in the satellite-derived aerosol products over the Tropics, though the interpretation in terms of actual aerosol behavior was ambiguous. *Tian et al.* [2011] further investigated the MJO-related aerosol variability over the tropical Atlantic Ocean using the aerosol optical thickness (AOT) product from the MODIS (Moderate Resolution Imaging Spectroradiometer) on the Aqua satellite. They suggested that the MJO-related intra-seasonal variance accounts for about 25% of the total AOT variance over the tropical Atlantic. They also found that the AOT anomalies are negatively correlated with the low-level zonal wind anomalies over most parts of tropical Atlantic, with the latter leading the former by about 6 days. This indicates the MJO may modulate Atlantic aerosol transport through its influence on the Atlantic low-level zonal winds. Given the potential predictability of the MJO extending to 2–4 weeks [e.g., *Waliser*, 2005], the study by *Tian et al.* [2011] implies that the Atlantic aerosol concentration may be predictable with lead times of 2–4 weeks, which in turn may lend important guidance to predicting air quality, dust storm activity, and ocean nutrient deposition over the Atlantic Ocean.

Nevertheless, *Tian et al.* [2011] examined only the total AOT anomalies and did not consider the contribution of different aerosol types to the total AOT anomalies. It is well known that the aerosol over the tropical Atlantic Ocean in the boreal winter season is a mixture of mineral dust from the Sahara desert and the Sahel region, biomass burning smoke from the Sahel and African savanna regions, and marine aerosol (primarily sea salt and secondly sulfate aerosols) from the ocean surface [*Kaufman et al.*, 2002; 2005a; 2005b]. Since dust, biomass burning smoke and marine aerosols play very different roles in the radiative forcing and cloud formation process, it is of great interest to partition the total aerosol into individual aerosol components and examine the MJO-related variability in each aerosol type.

Previous studies [*Kaufman et al.*, 2002; 2005a; 2005b] have suggested that satellite data distinguishing fine-mode aerosols from coarse-mode aerosols could be used to separate the aerosol into specific types, since different aerosol types (e.g., smoke, dust, and maritime sea salt aerosols) have different fine mode fraction (FMF) values. FMF is the fraction of total AOT contributed by the fine-mode aerosols. For example, smoke from wildfire biomass burning and urban-industrial air pollution from human combustion processes are dominated by fine-mode particles. On the other hand, desert dust and sea salt, mainly a result of wind and erosion processes, have a much larger proportion of coarse-mode particles. *Kaufman et al*. [2002; 2005a; 2005b] first demonstrated the usefulness of combining the total AOT and FMF measurements from MODIS/Terra to estimate dust and biomass burning smoke AOT components (see detailed description in section 2). This method has since been widely adopted by the community to understand aerosol types and their climate forcing [*Bellouin et al.*, 2005, among many others].

Measuring the reflectance of a target from different directions is very useful because geophysical media, for example aerosols, reflect solar light differently in different directions. The variations between the reflectances acquired from a variety of observation angles can be interpreted (with appropriate models) in terms of aerosol properties such as particle size, shape, and single-scattering albedo [*Kahn et al.*, 1998, 2001; *Chen et al.,* 2008]. In particular, MISR's sensitivity to the characteristics of the aerosol scattering phase functions enables it to distinguish between the non-spherical and spherical particles, and thus provides a possible way to separate mineral dust aerosols from other aerosol components. A series of studies has explored the ability of MISR to retrieve mineral dust properties theoretically [*Kahn et al.*, 1997, 2001; *Kalashnikova et al.*, 2005; *Kalashnikova and Kahn*, 2006], the sensitivity of the theoretical results, as well as the application of non-spherical dust models for five Saharan dust field events over the Atlantic Ocean [*Kalashnikova and Kahn*, 2008].

In this study, we use MODIS FMF to separate the total column AOT into its individual types over the tropical Atlantic, especially the dust and biomass burning smoke aerosols, because of its more frequent sampling. We will also use MISR aerosol non-spherical fraction to derive the dust aerosol component because of its greater particle type information content, and compare it with that derived from MODIS. The resulting intra-seasonal variabilities associated with the MJO in dust and biomass burning smoke aerosols over the tropical Atlantic Ocean are then examined.

The rest of this paper is organized as follows. Section 2 describes the MODIS and MISR data, and the methodology used to derive specific aerosol components from the total AOT. The climatology of specific aerosol component as well as the comparison of dust aerosol between MODIS and MISR is presented in Section 3 in order to examine the fidelity of the methods described in Section 2. The main results of this paper, the MJO-related dust and smoke aerosol anomalies, are presented in Section 4. Conclusions and discussions are presented in Section 5.

2. Methodology and Data Description

2.1. MODIS

2.1.1. Method to Calculate Dust, Smoke AOT

The method developed by *Kaufman et al*. (2005a, b) to derive the AOTs for dust and biomass burning smoke using MODIS total AOT and FMF measurements is briefly described as below. Over the tropical Atlantic Ocean during the boreal winter season, the aerosol is a mixture of dust, biomass burning smoke, and marine aerosols. Note that the term 'anthropogenic aerosol' in *Kaufman et al.*'s papers is replaced by 'biomass burning smoke' as the latter is far more appropriate term for the region of study. However, the 'smoke' does include a small contribution from air pollution that originates primarily from the US and South American continents. With the two constraints that both the total AOT and its fine model fraction can be partitioned into contributions from the dust, smoke, and marine aerosol components, we have the following equations:

$$\tau = \tau_{dust} + \tau_{smoke} + \tau_{mar} \quad (1)$$

$$f \times \tau = f_{dust} \times \tau_{dust} + f_{smoke} \times \tau_{smoke} + f_{mar} \times \tau_{mar} \quad (2),$$

in which τ and f denote AOT and FMF respectively (τ and AOT as well as f and FMF are interchangeable in this paper), and the subscripts 'dust', 'smoke', and 'mar' indicate dust, smoke, and marine aerosol component, respectively. Rewriting (1) and (2), we get

$$\tau_{dust} = [\tau\times(f_{smoke}-f)-\tau_{mar}\times(f_{smoke}-f_{mar})]/(f_{smoke}-f_{dust}) \quad (3)$$

$$\tau_{smoke} = [\tau\times(f-f_{dust})-\tau_{mar}\times(f_{mar}-f_{dust})]/(f_{smoke}-f_{dust}) \quad (4).$$

With τ and f being MODIS measurements, τ_{dust} and τ_{smoke} can be computed directly if f_{dust}, f_{smoke}, f_{mar}, and τ_{mar} are known.

In *Kaufman et al.*'s study, the FMFs of dust, smoke, and marine aerosols are assumed to be constant, and were derived by averaging the MODIS/Terra FMF measurements over selected regions and time periods where one specific aerosol type dominates, with their uncertainties estimated from these selected measurements: f_{dust}=0.5±0.05, f_{smoke}=0.9±0.05, and f_{mar}=0.3±0.1 [2005b]. However, the actual FMF values vary with season and location [*Maring et al.*, 2003; *Jones and Christopher*, 2007, 2011; *Yu et al.*, 2009], thus large uncertainties are expected from using constant f_{dust}, f_{smoke}, f_{mar} when applying Kaufman's formula. More discussion on this issue as well as the sensitivity of our results to the FMF values will be given in Section 4.3.

The marine AOT, τ_{mar}, depends strongly on surface wind speed as its primary component is sea-spray salt [e.g., *Smirnov et al.*, 2003]; it is estimated using the empirical formula in *Kaufman et al*. [2005b]:

$$\tau_{mar} = 0.007W+0.02 \quad (5)$$

Here, W is the surface (10 meter) wind speed from the ECMWF ERA-Interim reanalysis [*Dee et al.*, 2011]. The global mean of τ_{mar} is around 0.06±0.005 [e.g., *Kaufman et al.*, 2001].

2.1.2. MODIS Data Description

MODIS instruments are operating on both the Terra and Aqua satellites. Each has a viewing swath width of 2,330 km and views the entire surface of the Earth every one to two days. In this study, daily AOT and FMF measurements at 0.55 μm from the MODIS/Aqua Level-3 Collection 5.1 dataset [*Levy et al.*, 2009] on $1^{\circ} \times 1^{\circ}$ spatial grids are used. The uncertainties of τ are $\pm (0.03 + 0.05\tau)$ over ocean and $\pm (0.05 + 0.15\tau)$ over land. In MODIS, the fine-mode aerosols refer to the aerosols with a size distribution of radii centered between 0.1 and 0.25 μm, whereas the coarse-mode aerosols refer to those with a size distribution of radii centered between 1 and 2.5 μm. Validation studies indicate that, over ocean, the uncertainties of f are large for low AOT ($\tau<0.15$) but typically less than about 20% for large AOT ($\tau>0.15$) [*Kleidman et al.*, 2005; *Remer et al.*, 2005]. Over land, MODIS does not provide any quantitative information about the aerosol size [*Levy et al.*, 2010]. As a result, we use the τ and f data over the ocean only. The period of 4 July 2002 to 1 June 2009 is used for consistency with the study by *Tian et al*. [2011].

Note that we use MODIS/Aqua aerosol data rather than MODIS/Terra data even though MISR is on board Terra. One reason is that we want to be consistent with the study in *Tian et al.* [2011]. More importantly, MODIS/Terra and MISR aerosol retrievals are much less spatially overlapped due to the exclusion of sun glint regions over the ocean in MODIS. As a result there are many fewer days on which both MODIS/Terra and MISR made observations of a given region, compared to the situation between MODIS/Aqua and MISR. Since the direct comparison between daily MODIS and MISR aerosol data serves as an essential part of this study, we chose to use MODIS/Aqua data. The results based on MODIS/Terra were compared with those based on MODIS/Aqua, and it is found that the difference is negligible for our application.

2.1.3. MODIS Data Rejection

In this work, some MODIS τ and f measurements are rejected in our calculations for the reasons described below.

The dependence of τ_{dust} and τ_{smoke} on τ and f based on equations (3) and (4) is illustrated in Figure 1, where τ_{mar} is set to 0.06 (the approximate global mean value of τ_{mar}). It is seen that the larger the τ, the larger τ_{dust} and τ_{smoke}. Also, as f increases, τ_{smoke} increases and τ_{dust} decreases. Figure 1 also suggests that equations (3) and (4) can produce reasonable (nonnegative) values for both τ_{dust} and τ_{smoke} only when the paired τ and f measurements fall within a limited region bounded by the white dashed lines (τ_{dust}=−0.03 and τ_{smoke}=−0.03). We relax the limit of τ_{dust} or τ_{smoke} to −0.03 instead of 0 because the uncertainties of the MODIS AOT are ±0.03 over ocean, thus a small negative AOT up to -0.03 is regarded as indistinguishable from the value 0 [*Remer et al.*, 2005]. Note that calculated τ_{dust} and τ_{smoke} in the range of 0 to -0.03 have been set to zero. Outside this region, either τ_{dust} or τ_{smoke} is too negative, and correspondingly, τ_{smoke} or τ_{dust} would be larger than the total AOT, which is not physical. Therefore, the τ and f measurements giving rise to such τ_{dust} and τ_{smoke} values are rejected. In addition, τ measurements greater than 2 are excluded, given the large uncertainties from cloud contamination [*Zhang et al.*, 2005].

The count distribution of paired MODIS τ and f measurements as a function of τ and f is summarized for the tropical Atlantic (20°S – 30°N, 60°W – 20°E) and for the

2002–2009 boreal winters (October to April) in Figure 2a. It is found that the majority of observations fall within the region bounded by two lines ($\tau_{dust} = -0.03$ and $\tau_{smoke} = -0.03$); however, there is also a large number of observations falling outside the two lines, which are rejected in the calculation. The rejection results from both the limitations in MODIS data and the limitations in Kaufman's method. For example, in some cases τ is typically between 0.1–0.3, which is much larger than the baseline τ_{mar}, while f is extremely small, nearly 0 (see bottom of Figure 2a). These observations are very likely artifacts of cloud contamination [e.g., *Zhang et al.*, 2005; *Tian et al.*, 2008]. For other cases, τ is also significantly larger than τ_{mar} and f falls between f_{mar} and f_{dust}, suggesting the aerosol is a mixture of dust and sea salt (see the area between the line of τ_{smoke}=−0.03 and the line of f_{mar}). These are likely valid observations; however, due to the difficulties in separating dust from sea salt over this regime [*Kaufman et al.* 2005b], we don't include these observations in our calculations.

The percentage of days with MODIS τ and f measurements available relative to the total days during 2002–2009 boreal winters (1269) is shown in Figure 2b. The occurrence of cloudy conditions affecting the retrieval of MODIS aerosol parameters is evident, with the fraction of observations decreasing from more than 70% over the clear subtropical North Atlantic to about 35% over the cloudy equatorial Atlantic. After applying the data rejection described above, overall more than 50% of the observations remain. The most frequent rejections occur over the subtropical oceans, possibly due to the ambiguity between sea salt and dust aerosol over those regions

It is noted that we applied *Kaufman et al.*'s formula in a stricter way than what was originally done by *Kaufman et al.* [2005a and 2005b]. In *Kaufman et al.* [2005a]

when computing τ_{smoke}, they set negative τ_{smoke} values to zero, regardless of their magnitude. And in *Kaufman et al.* [2005b], when computing τ_{dust}, f is forced to be bounded within f_{dust} and f_{smoke} by setting any f values outside the bounds to the limiting values, to guarantee τ_{dust} is always positive. In our work, we include only those observations that fit the formula well. Nevertheless, it should be noted that although the data rejection we applied removes a large number of suspicious observations, doing so does not in itself guarantee the accuracy of the remaining applications, given that f_{dust}, f_{smoke}, and f_{mar} are assumed constant, and τ_{mar} was estimated from an empirical formula. For the former factor, sensitivity tests will be performed to examine the extent to which our results are sensitive to the variations in FMF values. For the latter, the deviations of the actual τ_{mar} (mainly sea salt) compared to that empirically computed will be interpreted primarily as changes in dust amount, thus affecting the accuracy of τ_{dust}. However, as will be presented next, MISR can distinguish dust from sea salt based on retrieved particle shape, thus τ_{dust} derived from MISR is not subject to the ambiguity between dust and sea salt that affects Kaufman's method. In this sense the examination of MISR aerosol observations provides validation for the more extensive MODIS data set, in addition to offering actual results independent of MODIS.

2.2. MISR

The MISR instrument aboard the Terra satellite views Earth in four spectral bands in each of nine view angles spread out in the forward and aft directions along the flight path at 70.5°, 60.0°, 45.6°, 26.1°, and nadir. With a swath about 360 km wide, global coverage with MISR is acquired about once every 9 days at the equator and 2 days toward the poles. Data collected from all nine viewing angles provide independent constraints on aerosol properties, separating mineral dust aerosols from other aerosol components operationally [*Kahn et al.*, 2010].

Assuming the mineral dust is all non-spherical and the non-spherical part of AOT is all from dust, MISR τ_{dust} can be directly computed as the non-spherical fraction of the total AOT:

$$\tau_{dust} = \tau \times f_{non\text{-}spherical} \qquad (6).$$

In MISR, smoke and marine aerosols (both sea salt and sulfate aerosols) contribute to the spherical part of the total AOT. (Refer to Table 3 in *Kahn et al.* [2001] for more details on shape categories of different aerosol components.) If τ_{mar} is again taken as computed from equation (5), τ_{smoke} can be approximated as the difference between the total τ and τ_{dust} and τ_{mar}:

$$\tau_{smoke} = \tau - \tau_{dust} - \tau_{mar} \qquad (7).$$

However, it should be kept in mind that unlike MISR τ_{dust}, the MISR τ_{smoke} derived this way, and all the MODIS particle type distinctions, are not independent observations based on actual physical constraints, and their accuracy is subject to the large uncertainties due to the empirically calculated τ_{mar}.

We use MISR-derived Level 3 daily τ and non-spherical fraction at 0.558 μm on 0.5º × 0.5º spatial grids during the same time period as the MODIS data. MISR τ and τ_{dust} are interpolated onto 1º × 1º grids to compare with MODIS results. A number of validation studies have shown that overall, about 70% to 75% of MISR AOT retrievals fall within 0.05 or 20%×AOT, and about 50% to 55% are within 0.03 or 10%×AOT, except at sites where mixed dust and smoke are commonly found [*Kahn et al.*, 2010].

Particle property validation suggests that expected MISR sensitivity to the spherical versus non-spherical particles is about 20% for AOT above 0.15, and diminishes for mid-visible AOT below this value [*Kahn et al.*, 1997; *Kalashnikova* et al., 2005; *Kalashnikova and Kahn*, 2006]. Thus we only use $\tau \geq 0.15$ to calculate τ_{dust} from equation (6). With this τ cutoff, it is found that more than 70% of the observations still remain for calculation over most of the tropical Atlantic (Figure 3b). Note generally MISR τ retrievals are available for about 15% of the time, except over the convectively active regions (decreased to about 10%, Figure 3a). Note also that although it is never been explicitly addressed, MODIS sensitivity to particle properties, e.g. FMF, also diminishes at low AOT (implied in Figure 7 in *Kahn et al.* [2009]), and MISR actually has greater sensitivity at low AOT than MODIS due to the long atmospheric paths observed by its steeper-viewing cameras.

Note that MISR also retrieves aerosol particle size information, thus conceptually it is possible to follow the same method utilized for MODIS to separate the total AOT into specific types in MISR. However MISR categorizes the aerosol particles into three bins: "fine" (particle radii<0.35um), "medium" (radii between 0.35 and 0.7), and "large" (radii >0.7um) modes, instead of two bins as "fine" vs. "coarse" in MODIS. Thus applying Kaufman's formula to MISR would require considerable additional work, but not necessarily lead to greater insight, because similar assumptions would be required to apply the size-discrimination method to MISR as to MODIS. Furthermore, the different radii range for MODIS and MISR "fine" mode would make it impossible to cross-validate the FMF values between these two datasets. Therefore, using MISR aerosol size information to separate different aerosol components following Kaufman's method is considered beyond the scope of current paper.

3. Comparison of Aerosol Components between MODIS and MISR

In this section, the AOTs of individual aerosol components over the tropical Atlantic Ocean are examined, and the MODIS and MISR results are compared. Climatological maps are examined first, in order to investigate how well the methods presented in Section 2 capture the basic features of the long-term mean.

3.1. Aerosol Winter Climatology

3.1.1. MODIS

The MODIS climatological mean (2002–2009) boreal winter (November to April) aerosol maps over the tropical Atlantic Ocean for τ, τ_{dust}, τ_{smoke}, and τ_{mar}, as well as their percentages relative to τ, are shown in Figure 4. The climatological mean τ features a zonally oriented, optically thick aerosol plume centered at around 5°N–8°N stretching across the equatorial Atlantic Ocean. The magnitude and latitudinal extent are greatest over the eastern equatorial Atlantic along the west coast of Africa and gradually decrease westward toward the central and western equatorial Atlantic, as expected for an aerosol plume that originates in Africa (Figure 4a). Note that this map is similar to Figure 1b (color shaded area) in *Tian et al.* [2011], but is not identical, due to the data rejection performed in this study. The magnitude of τ in Figure 4a is about 80% of that in *Tian et al.* [2011] over the heavy aerosol loading region (τ>0.15), and comparable over the clean subtropical Atlantic. Nevertheless, their overall patterns are similar, with spatial correlation as high as 0.98. The spatial pattern of climatological τ_{dust} resembles the τ pattern greatly, with maximum τ_{dust} found along the west coast of Africa (about 0.35) and a gradual decrease toward the central and western equatorial Atlantic (Figure 4b). Over the equatorial Atlantic Ocean, where aerosol loading is high (τ>0.15), dust is the dominant aerosol component, contributing greater than 50%, and as much as 75%, to τ (Figure 4c).

Compared to τ_{dust}, τ_{smoke} is significantly weaker. Plumes of fine-mode-dominant aerosol are found originating from the African (biomass burning smoke) as well as the South American continents (air pollution) (Figure 4d). A contribution of more than 20% to total τ is found over the eastern tropical Atlantic, while less than 20% over the western part (Figure 4e). Figure 4f shows that τ_{mar} is very small (about 0.04) over the Atlantic intertropical convergence zone and the west coast of Africa because of the weak trade winds. Over the clean subtropical Atlantic, marine aerosol is the dominant component (>50%) due to lack of dust and smoke aerosols over these regions.

These results indicate that the major aerosol plume over the equatorial Atlantic Ocean in Figure 4a is the dust originating in the Sahara desert and the Sahel region, with some contribution of biomass burning smoke originating in the Sahel and African savanna. These aerosol distributions are generally consistent with previous observational results [e.g., *Husar et al.*, 1997; *Kaufman et al.*, 2005b; *Huang et al.*, 2010a], lending some confidence to the quantitative assessment of the relative dust, smoke and marine AOTs contributions to the total AOT from equations (3) and (4) from MODIS.

3.1.2. MISR

MISR winter climatologies of τ, τ_{dust}, and τ_{smoke} are shown in Figure 5. Recall that for these results only cases with $\tau \geq 0.15$ are used due to the fact that sensitivity to shape diminishes when aerosol concentration is low. Data rejection is also applied to MODIS τ, too, as discussed in Section 2.1.3. Thus, we don't expect Figure 5a to be the same as

Figure 4a. Nevertheless, we do find they have highly consistent spatial patterns and comparable magnitudes. The climatological MISR τ_{dust} map (Figure 5b) is also very similar to the MODIS τ_{dust} (Figure 4b). The MISR τ and τ_{dust} are slightly larger than the MODIS counterparts partly due to MISR's exclusion of low aerosol cases, but more important reasons will be addressed in Section 3.2. It is seen that MISR τ_{dust} contributes more than 40%, up to more than 60%, to the total τ for cases with $\tau \geq 0.15$, further confirming that dust is the dominant aerosol component over the equatorial Atlantic Ocean (Figure 5c). It is also noted that MISR has 10% to 15% lower dust fraction over the equatorial Atlantic. Again, this difference could be partly attributed to the τ cutoff in MISR, but more importantly could result from both uncertainties involved in the derivation of MODIS and MISR τ_{dust}, especially in MODIS, given the assumptions used. This point will be discussed again in Section 3.2. The climatological MISR τ_{smoke}, calculated as described in Section 2.2, has a 10% larger contribution to total τ than MODIS τ_{smoke} over the equatorial Atlantic (Figure 5d and 5e compared to Figure 4d and 4e).

The overall consistency between the MODIS and MISR aerosol climatology gives us confidence in applying two independent satellite datasets and methods to derive the dust and smoke aerosols over the tropical Atlantic Ocean. However, the consistency in climatology does not guarantee their consistency on shorter time scales, for example, on the intra-seasonal time scale of importance here. Therefore, in next subsection we directly compare the coincident daily MODIS and MISR τ_{dust} over the tropical Atlantic Ocean.

3.2. Comparison of Coincident MODIS and MISR Dust Aerosols

In order to compare the daily τ_{dust} derived from MODIS and MISR, the correlation between them for all their coincident days during 2002-2009 over the tropical Atlantic is calculated. Here, the term "coincident" simply means the MODIS and MISR observations fall within a same grid box and on a same day, which is less strict than its usual implication used by the satellite community. We use the whole years for 2002-2009 instead of winters only in order to obtain as many coincident days as possible. The correlation is only calculated when there are at least five coincident days at a grid point.

Figure 6a shows that overall the MODIS and MISR dust AOTs are well correlated. The correlation is systematically higher in the north Atlantic region than that in the south, with more coincident days over the north Atlantic (Figure 6b). Over the North Atlantic, the correlation coefficient is typically around 0.7 or larger, whereas over the South Atlantic, the correlation is typically less than 0.5 with quite a few spots less than 0.2, or even negative. Generally, the correlation is higher when it is closer to the African continent, and decreases gradually as the dust is transported away from the source of the dust load. These results suggest that the MODIS and MISR derived dust aerosols agree with each other quite well over heavy dust load regions, whereas they are less consistent over the regions with less frequent dust occurrence or small dust aerosol concentration.

Figure 6a shows that overall the MODIS and MISR τ_{dust} are highly correlated, however the correlation coefficient does not provide information on the τ_{dust} magnitude. Therefore, the time series of MODIS and MISR τ_{dust} as the function of their coincident days at a representative grid point (29.5 W, 19.5 N), as well as averaged within the 5 × 5 and 10 × 10 gird boxes centered at this point, are shown (Figure 6c-e). Again it is found that the MODIS and MISR τ_{dust} are highly correlated on the daily basis, and it also reveals that τ_{dust} is systematically greater for MISR than MODIS.

MISR τ_{dust} is larger than MODIS τ_{dust} over most of the tropical Atlantic when averaged for coincident days (about 0.03 larger averaged over the basin), except in some regions north of the Equator (Figure 7b). This difference can be traced back to the difference between MISR and MODIS total AOT (Figure 7a). Over almost the entire tropical Atlantic, coincident MISR AOTs are systematically larger than the MODIS ones (up to 0.08, and about 0.04 when averaged for the Atlantic basin). This is consistent with previous studies in which MISR AOT is found to be generally larger than MODIS AOT over water [e.g., *Abdou et al.*, 2005; *Kahn et al.*, 2010]. Further examination of coincident MODIS and MISR τ and τ_{dust} binned against the MISR τ reveals that larger MISR τ is found for the entire τ spectrum, whereas MISR τ_{dust} is larger (smaller) when the aerosol concentration is relatively low (high) (Figure 7c). Note that lower aerosol concentrations are overwhelmingly more frequent (black line in Figure 7c), thus the averaged MISR τ_{dust} is larger than the averaged MODIS τ_{dust}. As seen above, the τ_{dust} difference between MODIS and MISR can be traced back to the τ difference between them. However, this is not the only reason, as, unlike MISR τ, MISR τ_{dust} is not systematically larger than MODIS τ_{dust}. The uncertainties involved in the derivation of both MODIS and MISR τ_{dust} inevitably lead to their differences too. However it should be noted that although both methods have limitations, MISR discrimination of aerosol type is much more robust than MODIS discrimination. The derivation of MISR τ_{dust} is based on actual retrieved particle property information, whereas for MODIS, the accuracy of the formula is subject to the use of constant FMF values and empirically calculated τ_{mar}. Despite more physically robust separation of τ_{dust} from τ in MISR, it has much less frequent sampling compared to MODIS, thus it is necessary to examine both datasets. Results based on these two complementary satellite datasets will provide more solid insight to the characteristics of the MJO-related dust and to some extent smoke variabilities.

4. MJO-related Atlantic Dust and Smoke AOT Anomalies

4.1. MJO Analysis Methodology

For the MJO analysis and composite procedure, we use the multivariate empirical orthogonal function (EOF) method introduced by *Wheeler and Hendon* [2004] and adopted widely by the MJO community [e.g., *Waliser et al.*, 2009]. Briefly, the intra-seasonal anomalies of daily AOT are obtained by removing the climatological-mean seasonal cycle and filtering via a 30–90-day band pass filter. Then, a composite MJO cycle (8 phases) is calculated by averaging the daily anomalies that occur within each phase of the MJO cycle. The MJO phase for each day is determined by the Real-time Multivariate MJO (RMM) index (a pair of PC time series called RMM1 and RMM2). Only days having strong MJO activity ($RMM1^2+RMM2^2>=1$) are considered.

Figure 8 shows the number of strong MJO days, or events ($RMM1^2+RMM2^2>=1$), used for the 8-phase MJO cycle composite for both MODIS and MISR during 2002–2009 boreal winters. The number of total strong MJO events for each MJO phase during this period is also shown at the right upper corner of each panel. For both instruments, the number of strong MJO events used for the composite is much less than the actual number of total events because of satellite retrieval sampling issues and the data rejection applied. Generally, the number of MODIS events ranges from about 10 to 45, about as three times more than MISR, due to the much wider MODIS swath.

4.2. MODIS and MISR

The 8-phase MJO composite maps of MODIS total τ, τ_{dust} and τ_{smoke} anomalies are shown in Figure 9a, 10a and 11a, respectively. The MISR counterparts will be discussed and compared with MODIS results later in Section 4.4. Comparing Figure 9a and 10a, it is seen that MODIS τ and τ_{dust} have very similar temporal evolution and spatial patterns, except that τ_{dust} anomalies are slightly smaller. The spatial correlation between τ and τ_{dust} anomalies for 8 MJO phases is 0.89. For both τ and τ_{dust}, strong negative anomalies (as large as about -0.04) are found over the entire equatorial Atlantic for MJO phases 1, 2, 3, and 8. In contrast, strong positive anomalies (up to 0.04) are found over the equatorial Atlantic for MJO phases 5–6. For MJO phase 4, strong positive anomalies occur to the north of the equator, whereas negative τ anomalies are found to the south. The converse is true for the MJO phase 7. The MJO composite maps of total τ greatly resemble those shown by *Tian et al.* [2011], with spatial correlation 0.52 (significant at the 99.9% level), and have very similar magnitudes. This resemblance suggests that the MJO-related total AOT anomaly patterns are robust and not sensitive to the data sampling (fewer samples are used in this study). The MJO-related τ_{smoke} anomalies in MODIS are very weak, rarely exceeding 0.01(Figure 11a). The spatial correlation between τ_{smoke} and τ is only about 0.21. The MJO composite maps of τ_{mar} anomalies are not shown since τ_{mar} is linearly dependent on the surface wind speed, thus the MJO-related τ_{mar} anomaly pattern in fact reflect the wind anomalies associated with the MJO, which has been examined in *Tian et al.* [2011]. Furthermore, it is found that the magnitudes of the τ_{mar} anomalies are negligible: the strongest negative/positive anomalies are about -0.004/0.004 (figure not shown).

The 8-phase MJO composite maps of MISR total τ, τ_{dust} and τ_{smoke} anomalies are shown in Figures 9b, 10b and 11b. Again, it is found that the τ_{dust} anomalies are significantly larger than the τ_{smoke} anomalies. The τ_{dust} anomalies have very similar patterns to those of total τ, with slightly smaller magnitude, whereas the τ_{smoke} anomalies are very small and noisy. Further comparison between the MISR and MODIS τ and τ_{dust} results (Figures 9 and 10) indicates that overall they exhibit very similar temporal evolution as well as anomaly patterns despite the systematically larger MISR anomalies compared to those of MODIS, which is likely the outcome of the systematically larger MISR τ and τ_{dust} retrievals compared to MODIS over the tropical Atlantic Ocean, as discussed earlier. The rejection of all $\tau < 0.15$ data in MISR could contribute to the above difference, too; however, MISR τ anomalies with no data rejection don't show evident differences (Figure not shown). Besides the magnitude difference, MISR τ and τ_{dust} anomalies are also noisier than the MODIS anomalies due to lower sampling. Nevertheless, the consistency between the MODIS and MISR results shown in Figures 9-11 demonstrate that dust is the dominant aerosol component on the intra-seasonal time scale, and the MJO-related dust anomalies are robust, as seen from two independent sets of satellite observations with different strengths and limitations.

4.3. Sensitivity of MODIS Results

Kaufman et al.'s method to compute τ_{dust} and τ_{smoke} using MODIS τ and f based on equations (3) and (4) is straightforward; however, large uncertainties in the computed τ_{dust} and τ_{smoke} are expected for at least several reasons: the uncertainties in the MODIS τ and f retrievals, the uncertainties in empirically computed τ_{mar}, and most critically, the uncertainties resulted from assuming constant f_{mar}, f_{dust}, and f_{smoke}. In this subsection, we will examine the sensitivity of our results to the FMF values. We first perturb the FMF values used in this study (see Section 2.1.1) by increasing/decreasing one of them at a time by its uncertainty range while keeping the other two unchanged. These sensitivity test cases are denoted group 1. We then test using FMF values derived by three other studies [*Jones and Christopher*, 2007; 2011; *Yu et al.*, 2009], which are denoted group 2. These studies have attempted to calibrate Kaufman's technique, and re-derived the FMFs using either updated MODIS datasets, or aerosol observations from other satellite datasets, or using the GOCART (Goddard Chemistry Aerosol Radiation and Transport) model to locate regions where a single aerosol component dominates. The FMF values they obtained are generally consistent with what is used in this study: f_{mar}, f_{dust}, and f_{smoke} are 0.25, 0.44, and 0.83, respectively in the study by *Jones and Christopher* [2007], and 0.31, 0.49, and 0.78 in their 2011 study, and 0.45, 0.37, and 0.90 in *Yu et al.* [2009]. FMFs do vary, and these studies find that they vary considerably depending on region and season.

Figure 12a shows the composite 8-phase MJO cycles of τ_{dust} anomalies averaged over the equatorial Atlantic (30 W–15 W, EQ–15 N) based on different sensitivity test cases. The 30 W–15 W, EQ–15 N box is chosen to represent the region with strong intra-seasonal aerosol variations. Overall, the colored lines (9 sensitivity tests) cluster around the solid black curve (control case), and the MJO cycles of τ_{dust} anomalies based on different sensitivity tests show a coherent evolution. This suggests that the MJO associated τ_{dust} anomalies over the tropical Atlantic are quite robust despite the uncertainties in using constant FMFs. Nevertheless, the lines spread in some phases. The result based on *Yu et al.* [2009] is most different from other cases, probably because in the other studies, the FMF values follow the sequence $f_{mar} < f_{dust} < f_{smoke}$ despite the deviations, whereas the order of f_{mar} and f_{dust} is reversed in *Yu et al.*'s study [2009]. The spread in group 2 is naturally larger than that in group 1. Furthermore, the τ_{dust} anomalies are more sensitive to f_{dust}, as indicated by the larger deviations of the dashed cyan and blue curves to the control case in phase 2, 3 and 6.

Similarly, Figure 12b shows the sensitivity test results for τ_{smoke} anomalies. The spread of τ_{smoke} anomalies is quite large compared to their magnitude. Nevertheless, the overall MJO cycle of τ_{smoke} anomalies is consistent among the different cases and their magnitudes are much smaller than that of the τ_{dust} anomalies.

5. Summary and Conclusions

Previous studies [*Tian et al.*, 2008; 2011] found significant intra-seasonal variability related to the MJO in the total column AOT over the tropical Atlantic region. Aerosol over the tropical Atlantic is primarily a mixture of mineral dust, biomass burning smoke, and marine aerosol. Given the different roles in the radiative forcing and cloud formation processes played by these three aerosol types, as well as the potential predictability of the MJO extending to 2–4 weeks, it is of great interest to further examine the MJO-related variability for individual aerosol types, especially dust and smoke aerosols.

Daily MODIS/Aqua total AOT and FMF measurements are used to derive daily τ_{dust} and τ_{smoke} following *Kaufman et al.*'s method [2005a, b]. This method contains considerable uncertainties, due to the assumption of constant f_{dust}, f_{smoke} , f_{mar} as well as the empirical calculation of τ_{mar}. Strict data rejection has been applied in order to use Kaufman's formula in a safer way. With MISR's sensitivity to aerosol particle shape, dust and smoke aerosols can be distinguished using the MISR aerosol non-spherical fraction. Because MISR sensitivity to shape (and MODIS sensitivity to FMF) diminishes when aerosol concentration is low, only $\tau >= 0.15$ data are used to compute $\tau_{\text{dust and Tsmoke}}$ for MISR. The examination of both datasets is necessary, and results from MODIS and MISR are complementary: MODIS provides better spatial coverage, and MISR dust is derived from actual aerosol property retrieval rather than assumed aerosol-type-specific FMF.

Both MODIS and MISR show a very similar dust and smoke winter climatology. τ_{dust} is found to be the dominant aerosol component over the tropical Atlantic. It is largest over the eastern equatorial Atlantic (about 0.35) and gradually decreases toward the west. τ_{smoke} is significantly smaller than τ_{dust}, Over the equatorial Atlantic with strong total aerosol loading, the contribution of τ_{dust} to total τ ranges from 40% to 70%, in contrast to about 25% is attributed to τ_{smoke} and less than 20% from τ_{mar}. The daily MODIS and MISR τ_{dust} are overall highly correlated, with the correlation coefficients typically about 0.7 over the North Atlantic, but much smaller or even negative over the South Atlantic. MISR τ_{dust} is found to be systematically greater than the coincident MODIS τ_{dust}, and this difference can be traced to the AOT difference between them. The consistency of the MODIS and MISR dust and smoke aerosol climatology and daily variations give us confidence to use these two data sets to investigate the relative contribution of dust and smoke aerosols to the total AOT variation associated with the MJO. However, the identification of smoke is much less certain than that of dust, because discrimination among fine-mode sea salt, sulfate, and smoke particles depends on assumptions for both MODIS and MISR, whereas the MISR dust discrimination is based on retrieved particle shape.

For MODIS, the MJO composite maps of τ_{dust} anomalies are very similar to those of τ anomalies, and are of comparable magnitude. Furthermore, the variance of τ_{dust} anomalies on the full intra-seasonal time scale is found to be comparable or even bigger than that of the τ anomalies. In contrast, the MJO-related τ_{smoke} anomalies are rather small, barely exceeding 0.01, and the τ_{mar} anomalies are negligible. The sensitivity study further shows that the MJO-related τ_{dust} and τ_{smoke} anomalies are quite robust, even when we perturb the FMFs by their uncertainty ranges or use different sets of FMFs from several independent studies.

Similarly, MISR also shows that the MJO composite maps of τ_{dust} anomalies are very similar to those of τ anomalies, while the MJO-related τ_{smoke} anomalies are rather small. The composite MJO cycle of τ_{dust} anomalies from MISR over the tropical Atlantic Ocean is consistent with the MODIS results although the anomalies are much noisier due to its less frequent sampling. The magnitude of MISR anomalies is again found to be systematically larger than that of MODIS. The MJO-related τ_{smoke} anomalies in MISR are overall slightly larger than for MODIS, but still much smaller compared to MISR τ_{dust} anomalies.

The consistency between the MODIS and MISR τ_{dust} and tsmoke anomalies in terms of the evolution of the MJO cycle as well as the spatial pattern of anomalies suggests that dust aerosol is the dominant component on the intra-seasonal time scale over the tropical Atlantic Ocean.

The observational results obtained from two complementary satellite datasets can be used to evaluate chemical transport models and help in model development.

Furthermore, given the potential predictability of the MJO, this study implies the MJO modulation of Atlantic dust aerosol concentration may be predictable with lead times of 2–4 weeks, which in turn may lend guidance to many other dust-related phenomena, such as the air quality, dust storm activity, and ocean nutrient deposition over the Atlantic Ocean.

Acknowledgments

This research was performed at Jet Propulsion Laboratory (JPL), California Institute of Technology (Caltech), under a contract with National Aeronautics and Space Administration (NASA). It was supported in part by the National Science Foundation (NSF) grant ATM-0840755 at University of California, Los Angeles. The work of R. Kahn is supported in part by NASA's Climate and Radiation Research and Analysis Program, under H. Maring, NASA's Atmospheric Composition Program under R. Eckman, and the EOS-MISR project. The MODIS/Aqua data used in this study have been obtained from the NASA LAADS server and ERA-Interim data used in this study have been obtained from the ECMWF Data Server.

References

Abdou, W. A., D. J. Diner, J. V. Martonchik, C. J. Bruegge, R. A. Kahn, B. J. Gaitley, K. A. Crean, L. A. Remer, and B. Holben (2005), Comparison of coincident Multiangle Imaging Spectroradiometer and Moderate Resolution Imaging Spectroradiometer aerosol optical depths over land and ocean scenes containing Aerosol Robotic Network sites, *J. Geophys. Res., 110*, D10S07, doi:10.1029/2004JD004693.

Bellouin, N., O. Boucher, J. Haywood, and M. S. Reddy (2005), Global estimate of aerosol direct radiative forcing from satellite measurements, *Nature, 438*(7071), 1138-1141, 10.1038/nature04348.

Chen, W-T, R. Kahn, D. Nelson, K. Yau, and J. Seinfeld (2008), Sensitivity of multi-angle imaging to optical and microphysical properties of biomass burning aerosols, *J. Geophys. Res.* 113, D10203, doi:10.1029/2007JD009414.

Dee, D. P., S. M. Uppala, A. J. Simmons, P. Berrisford, P. Poli, S. Kobayashi, U. Andrae, M. A. Balmaseda, G. Balsamo, P. Bauer, et al. (2011), The ERA-Interim reanalysis: Configuration and performance of the data assimilation system, *Q. J. Roy. Meteor. Soc., 137*(656), 553-597, 10.1002/qj.828.

Huang, J. F., C. D. Zhang, and J. M. Prospero (2010a), African dust outbreaks: A satellite perspective of temporal and spatial variability over the tropical Atlantic Ocean, *J. Geophys. Res., 115*, D05202, doi:10.1029/2009jd012516.

Husar, R. B., J. M. Prospero, and L. L. Stowe (1997), Characterization of tropospheric aerosols over the oceans with the NOAA Advanced Very High Resolution Radiometer optical thickness operational product, *J. Geophys. Res., 102*(D14), 16889-16909.

Jones, T. A., and S. A. Christopher (2007), MODIS derived fine mode fraction characteristics of marine, dust, and anthropogenic aerosols over the ocean, constrained by GOCART, MOPITT, and TOMS, *J. Geophys. Res., 112*(D22), D22204, doi:10.1029/2007jd008974.

Jones, T. A., and S. A. Christopher (2011), A reanalysis of MODIS fine mode fraction over ocean using OMI and daily GOCART simulations, *Atmos. Chem. Phys., 11*(12), 5805-5817, 10.5194/acp-11-5805-2011.

Kahn R.A., R. West, D. McDonald, B. Rheingans, and M. I. Mishchenko (1997), Sensitivity of Multi-angle remote sensing observations to aerosol sphericity, *J. Geophys. Res.*, 861-16,870, 102, 16

Kahn, R., P. Banerjee, D. McDonald, and D. J. Diner (1998), Sensitivity of multiangle imaging to aerosol optical depth and to pure-particle size distribution and composition over ocean, *J. Geophys. Res., 103*(D24), 32,195–32,213, doi:10.1029/98JD01752.

Kahn, R., P. Banerjee, and D. McDonald (2001), The sensitivity of multiangle imaging to natural mixtures of aerosols over ocean, *J. Geophys. Res., 106*(D16), 18,219–18,238, doi:10.1029/2000JD900497.

Kahn, R. A., B. Gaitley, J. Martonchik, D. Diner, K. Crean, and B. Holben (2005), MISR global aerosol optical depth validation based on two years of coincident AERONET observations. *J. Geophys. Res.*, doi: 10: 1029/2004JD004706.

Kahn, R.A., D.L. Nelson, M.Garay, R.C. Levy, M.A. Bull, D.J. Diner, J.V. Martonchik, S.R. Paradise, and E.G. Hansen, and L.A. Remer (2009), MISR Aerosol product attributes, and statistical comparisons with MODIS, IEEE Trans. Geosci. Remt. Sens 47, 4095-4114.

Kahn, R.A., B.J. Gaitley, M.J. Garay, D.J. Diner, T. Eck, A. Smirnov, and B.N. Holben (2010), MISR aerosol product assessment by comparison with AERONET, *J. Geophys. Res.*, doi: 10.1029/2010JD014601.

Kalashnikova O. V., R. A. Kahn (2008), Mineral dust plume evolution over the Atlantic from MISR and MODIS aerosol retrievals, *J. Geophys. Res., 113*, D24204, doi:10.1029/2008JD010083.

Kalashnikova, O. V., and R. Kahn (2006), Ability of multiangle remote sensing observations to identify and distinguish mineral dust types: Sensitivity over dark water, *J. Geophys. Res.,111*, D11207, doi:10.1029/2005JD006756.

Kalashnikova O. V., R. Kahn, I.N. Sokolik and W.-H Li (2005), The ability of multi-angle remote sensing observations to identify and distinguish mineral dust types: Optical models and retrievals of optically thick plumes, *J. Geophys. Res.,110*, D18S14, doi:10.1029/2004JD004550

Kaufman, Y. J., A. Smirnov, B. N. Holben, and O. Dubovik (2001), Baseline maritime aerosol: Methodology to derive the optical thickness and scattering properties, *Geophys. Res. Lett., 28*(17), 3251-3254.

Kaufman, Y. J., D. Tanre, and O. Boucher (2002), A satellite view of aerosols in the climate system, *Nature, 419*(6903), 215-223.

Kaufman, Y. J., O. Boucher, D. Tanre, M. Chin, L. A. Remer, and T. Takemura (2005a), Aerosol anthropogenic component estimated from satellite data, *Geophys. Res. Lett., 32*(17), L17804, doi 10.1029/2005gl023125.

Kaufman, Y. J., I. Koren, L. A. Remer, D. Tanre, P. Ginoux, and S. Fan (2005b), Dust transport and deposition observed from the Terra-Moderate Resolution Imaging Spectroradiometer (MODIS) spacecraft over the Atlantic ocean, *J. Geophys. Res., 110*(D10), D10s12, doi:10.1029/2003jd004436.

Kleidman, R. G., N. T. O'Neill, L. A. Remer, Y. J. Kaufman, T. F. Eck, D. Tanre, O. Dubovik, and B. N. Holben (2005), Comparison of moderate resolution imaging spectroradiometer (MODIS) and aerosol robotic network (AERONET) remote-sensing retrievals of aerosol fine mode fraction over ocean, *J. Geophys. Res., 110*(D22), D22205, doi:10.1029/2005jd005760.

Lau, W. K. M., and D. E. Waliser (Eds.) (2005), Intraseasonal Variability of the Atmosphere-Ocean Climate System, 474 pp., Springer, Heidelberg, Germany.

Levy, R. C., L. A. Remer, D. Tanré, S. Mattoo, and Y. J. Kaufman (2009), Algorithm for remote sensing of tropospheric aerosol over dark targets from MODIS: Collections 005 and 051, revision 2. MODIS algorithm theoretical basis document.

Levy, R. C., L. A. Remer, R. G. Kleidman, S. Mattoo, C. Ichoku, R. Kahn, and T. F. Eck (2010), Global evaluation of the collection 5 MODIS dark-target aerosol products over land, *Atmos. Chem. Phys., 10*(21), 10399-10420, 10.5194/acp-10-10399-2010.

Li, K. F., B. Tian, D. E. Waliser, and Y. L. Yung (2010), Tropical mid-tropospheric CO2 variability driven by the Madden-Julian oscillation, *Proc. Nat. Acad. Sci. USA., 107*(45), 19171-19175, 10.1073/pnas.1008222107.

Li, K.-F., Tian, B., Waliser, D. E., Schwartz, M. J., Neu, J. L., Worden, J. R., and Yung,

Y. L.: Vertical structure of MJO-related subtropical ozone variations from MLS, TES, and SHADOZ data, *Atmos. Chem. Phys. Discuss., 11*, 24503-24533, doi:10.5194/acpd-11-24503-2011, 2011.

Madden, R. A., and P. R. Julian (1971), Detection of a 40-50 day oscillation in the zonal wind in the tropical Pacific, *J. Atmos. Sci., 28*(7), 702-708.

Madden, R. A., and P. R. Julian (1972), Description of global-scale circulation cells in tropics with a 40-50 day period, *J. Atmos. Sci., 29*(6), 1109-1123.

Maring, H., D. L. Savoie, M. A. Izaguirre, L. Custals, and J. S. Reid (2003), Mineral dust aerosol size distribution change during atmospheric transport, *J. Geophys. Res., 108*(D19), 8592, doi:10.1029/2002jd002536.

Remer, L. A., Y. J. Kaufman, D. Tanre, S. Mattoo, D. A. Chu, J. V. Martins, R. R. Li, C. Ichoku, R. C. Levy, R. G. Kleidman, et al. (2005), The MODIS aerosol algorithm, products, and validation, *J. Atmos. Sci., 62*(4), 947-973.

Smirnov, A., B. N. Holben, T. F. Eck, O. Dubovik, and I. Slutsker (2003), Effect of wind speed on columnar aerosol optical properties at Midway Island, *J. Geophys. Res., 108*(D24), 4802, doi:10.1029/2003JD003879.

Tian, B., Y. L. Yung, D. E. Waliser, T. Tyranowski, L. Kuai, E. J. Fetzer, and F. W. Irion (2007), Intraseasonal variations of the tropical total ozone and their connection to the Madden-Julian Oscillation, *Geophys. Res. Lett., 34*(8), L08704, doi:10.1029/2007GL029451.

Tian, B., D. E. Waliser, R. A. Kahn, Q. Li, Y. L. Yung, T. Tyranowski, I. V. Geogdzhayev, M. I. Mishchenko, O. Torres, and A. Smirnov (2008), Does the Madden-Julian Oscillation influence aerosol variability?, *J. Geophys. Res.,* *113*(D12), D12215, doi:10.1029/2007jd009372.

Tian, B., and D. E. Waliser (2011), Chemical and biological impacts, Ch. 18 in Intraseasonal variability in the atmosphere-ocean climate system (2nd edition), edited by W. K. M. Lau and D. E. Waliser, Springer, Heidelberg, Germany.

Tian, B., D. E. Waliser, R. A. Kahn, and S. Wong (2011), Modulation of Atlantic aerosols by the Madden-Julian Oscillation, *J. Geophys. Res., 116*, doi:10.1029/2010JD015201.

Waliser, D., K. Sperber, H. Hendon, D. Kim, M. Wheeler, K. Weickmann, C. Zhang, L. Donner, J. Gottschalck, W. Higgins, et al. (2009), MJO simulation diagnostics, *J. Climate, 22*(11), 3006-3030, 10.1175/2008jcli2731.1.

Waliser, D. E. (2005), Predictability and forecasting, Ch. 12 in Intraseasonal Variability of the Atmosphere-Ocean Climate System, edited by W. K. M. Lau and D. E. Waliser, pp. 389-424, Springer, Heidelberg, Germany.

Weare, B. C. (2010), Madden-Julian Oscillation in the tropical stratosphere, *J. Geophys. Res., 115*, D17113, doi:10.1029/2009jd013748.

Wheeler, M. C., and H. H. Hendon (2004), An all-season real-time multivariate MJO index: Development of an index for monitoring and prediction, *Mon. Wea. Rev., 132*(8), 1917-1932, 10.1175/1520-0493(2004)132<1917:aarmmi>2.0.co;2.

Wong, S., and A. E. Dessler (2007), Regulation of H2O and CO in tropical tropopause layer by the Madden-Julian oscillation, *J. Geophys. Res., 112*(D14), D14305, 10.1029/2006jd007940.

Wong, S., A. E. Dessler, N. M. Mahowald, P. Yang, and Q. Feng (2009), Maintenance of lower tropospheric temperature inversion in the Saharan Air Layer by dust and dry anomaly, *J. Climate, 22*(19), 5149-5162, 10.1175/2009jcli2847.1.

Yu, H. B., M. Chin, L. A. Remer, R. G. Kleidman, N. Bellouin, H. S. Bian, and T. Diehl (2009), Variability of marine aerosol fine-mode fraction and estimates of anthropogenic aerosol component over cloud-free oceans from the Moderate Resolution Imaging Spectroradiometer (MODIS), *J. Geophys. Res., 114*, D10206, doi:10.1029/2008jd010648.

Zhang, C. (2005), The Madden-Julian Oscillation, *Rev. Geophys., 43*, RG2003, doi:10.1029/2004RG000158.

Zhang, J. L., J. S. Reid, and B. N. Holben (2005), An analysis of potential cloud artifacts in MODIS over ocean aerosol optical thickness products, *Geophys. Res. Lett., 32(15),* L155803, doi:10.1029/2005gl023254.

Figure Captions

Figure 1: Calculated a) τ_{dust} and b) τ_{smoke} as a function of total τ and f according to equations (3) and (4). Here, f_{mar}=0.3, f_{dust}=0.5, f_{smoke}=0.9, and τ_{mar}=0.06, as indicated by four white straight lines. The white dashed lines indicate $\tau_{dust}=-0.03$ and $\tau_{smoke}=-0.03$. Contour interval: 0.1.

Figure 2: a) The count of paired MODIS τ and f measurements with respect to τ and f over the tropical Atlantic (20°S–30°N, 60°W–20°E) for 2002–2009 boreal winters. Superimposed solid lines are the lines of $\tau_{dust}=-0.03$ and $\tau_{smoke}=-0.03$ in Figure 1. b) The percentage of days with MODIS τ and f measurements during 2002–2009 boreal winters (1269 days in total). c) The percentage of τ and f measurements used to calculate τ_{dust} and τ_{smoke} relative to the total number of measurements.

Figure 3: a) The percentage of days with MISR τ measurements during 2002–2009 boreal winters (1269 days in total). b) The percentage of MISR $\tau \geq 0.15$ relative to total number of τ measurements.

Figure 4: MODIS climatological mean (2002–2009) boreal winter a) total τ, b) τ_{dust}, d) τ_{smoke}, and f) τ_{mar} over the tropical Atlantic Ocean, as well as their percentages to τ (c-τ_{dust}, e-τ_{smoke}, and g-τ_{mar}). 9-point spatial smoothing is applied.

Figure 5: Same as Figure 3a-3e but for MISR, and only cases with MISR $\tau \geq 0.15$ used.

Figure 6: a) Correlation coefficients between coincident MODIS τ_{dust} and MISR τ_{dust} during 2002-2009 over the tropical Atlantic and b) the number of coincident days. Time series of MODIS (blue) and MISR (red) τ_{dust} as the function of the coincident day c) at the point of 29.5 W, 19.5 N, averaged on the d) 5 × 5 and e) 10 × 10 boxes centered at 29.5 W, 19.5 N.

Figure 7: a) MISR and MODIS τ difference averaged over coincident days during 2002-2009. b) Same as a), but for τ_{dust}. c) Number of coincident MODIS and MISR observations (black line), averaged MODIS τ (thick blue line), MISR τ (thick red line), MODIS τ_{dust} (thin blue line), and MISR τ_{dust} (thin red line) over 20°S–30°N, 60°W–20°E during 2002–2009 as a function of binned MISR τ (binned by every 0.01).

Figure 8: The number of strong MJO events used for MJO composite for each phase of the MJO cycle for a) MODIS and b) MISR during the 2002–2009 boreal winters. The total number of strong MJO events during this period is indicated at the right upper corner of each panel.

Figure 9: MJO composite maps of total τ anomalies (multiplied by 100) for a) MODIS and b) MISR over the tropical Atlantic Ocean. 9-point spatial smoothing is applied.

Figure 10: Same as Figure 9, but for τ_{dust}.

Figure 11: Same as Figure 9, but for τ_{smoke}.

Figure 12: The composite MJO cycle of MODIS a) τ_{dust} and b) τ_{smoke} anomalies averaged over 30 W–15 W, EQ–15 N for the control case (black) and 9 sensitivity test cases (color) with f_{mar}, f_{dust}, and f_{smoke} of each case indicated in the legend.

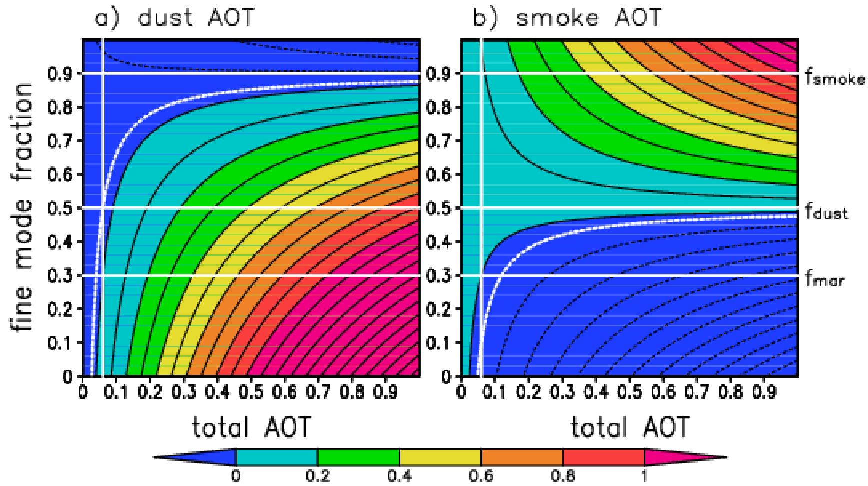

Figure 1: Calculated a) τ_{dust} and b) τ_{smoke} as a function of total τ and f according to equations (3) and (4). Here, f_{mar}=0.3, f_{dust}=0.5, f_{smoke}=0.9, and τ_{mar}=0.06, as indicated by four white straight lines. The white dashed lines indicate τ_{dust}=−0.03 and τ_{smoke}=−0.03. Contour interval: 0.1.

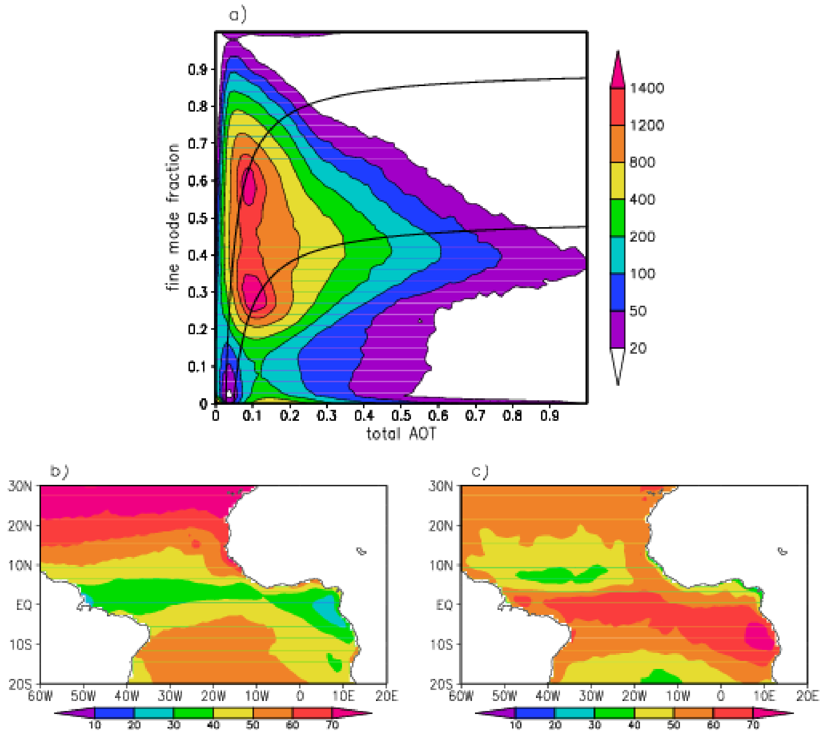

Figure 2: a) The count of paired MODIS τ and f measurements with respect to τ and f over the tropical Atlantic (20°S–30°N, 60°W–20°E) for 2002–2009 boreal winters. Superimposed solid lines are the lines of τ_{dust}=−0.03 and τ_{smoke}=−0.03 in Figure 1. b) The percentage of days with MODIS τ and f measurements during 2002–2009 boreal winters (1269 days in total). c) The percentage of τ and f measurements used to calculate τ_{dust} and τ_{smoke} relative to the total number of measurements.

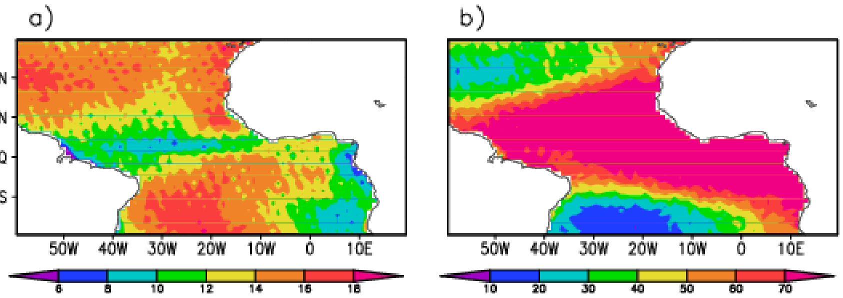

Figure 3: a) The percentage of days with MISR τ measurements during 2002–2009 boreal winters (1269 days in total). b) The percentage of MISR τ ≥ 0.15 relative to total number of τ measurements.

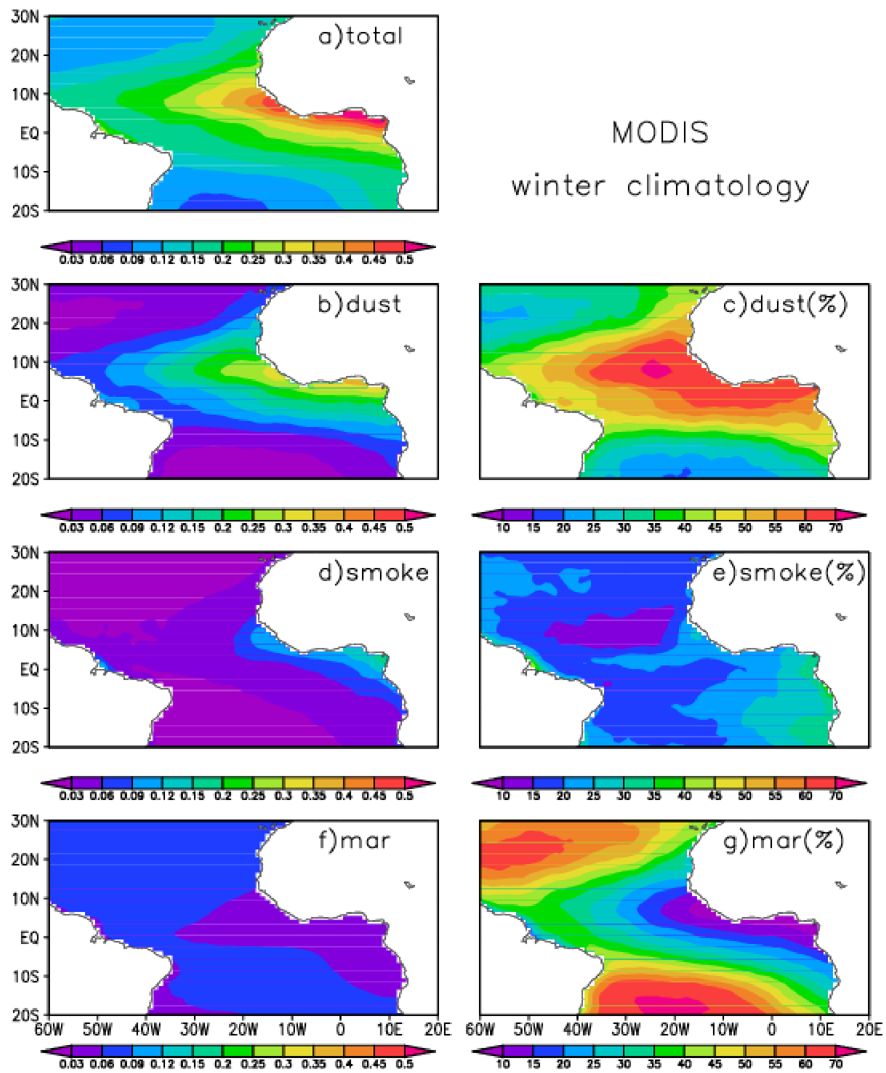

Figure 4: MODIS climatological mean (2002–2009) boreal winter a) total τ, b) τ_{dust}, d) τ_{smoke}, and f) τ_{mar} over the tropical Atlantic Ocean, as well as their percentages to τ (c-τ_{dust}, e-τ_{smoke}, and g-τ_{mar}). 9-point spatial smoothing is applied.

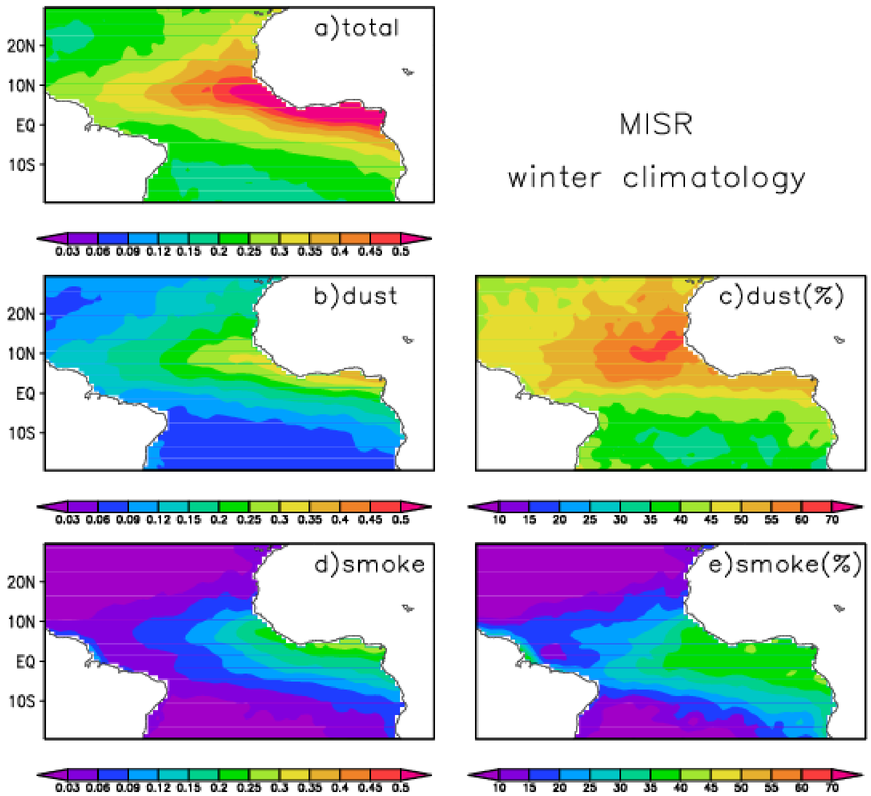

Figure 5: Same as Figure 3a-3e but for MISR, and only cases with MISR $\tau \geq 0.15$ used.

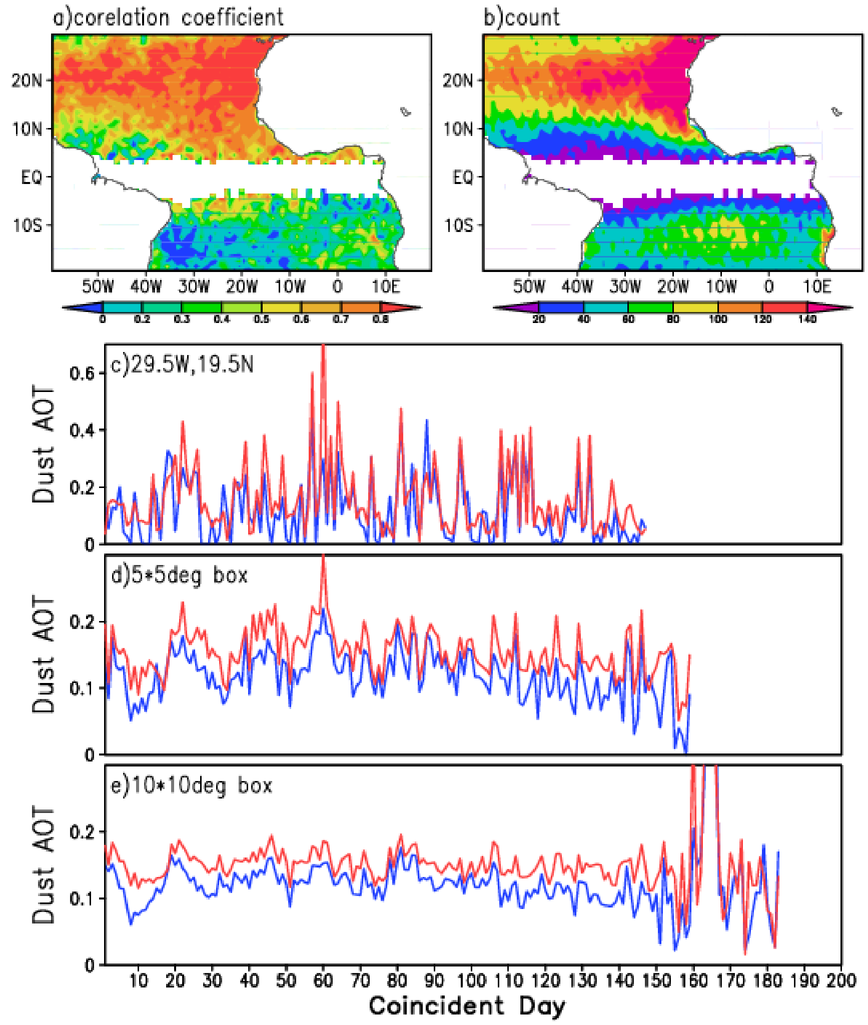

Figure 6: a) Correlation coefficients between coincident MODIS τ_{dust} and MISR τ_{dust} during 2002-2009 over the tropical Atlantic and b) the number of coincident days. Time series of MODIS (blue) and MISR (red) τ_{dust} as the function of the coincident day c) at the point of 29.5 W, 19.5 N, averaged on the d) 5 × 5 and e) 10 × 10 boxes centered at 29.5 W, 19.5 N.

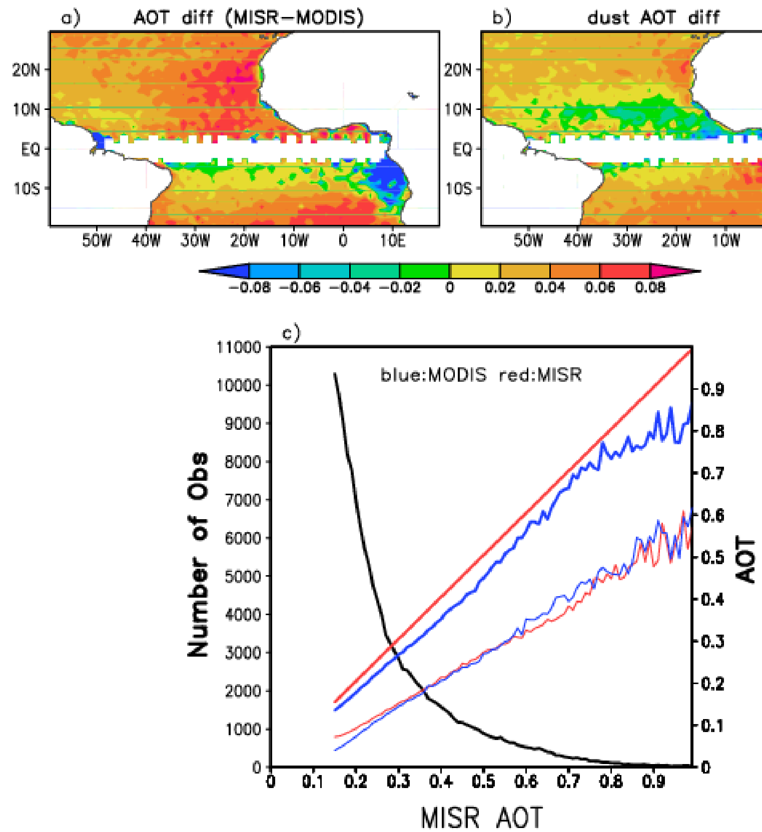

Figure 7: a) MISR and MODIS τ difference averaged over coincident days during 2002-2009. b) Same as a), but for τ_{dust}. c) Number of coincident MODIS and MISR observations (black line), averaged MODIS τ (thick blue line), MISR τ (thick red line), MODIS τ_{dust} (thin blue line), and MISR τ_{dust} (thin red line) over 20°S–30°N, 60°W–20°E during 2002–2009 as a function of binned MISR τ (binned by every 0.01).

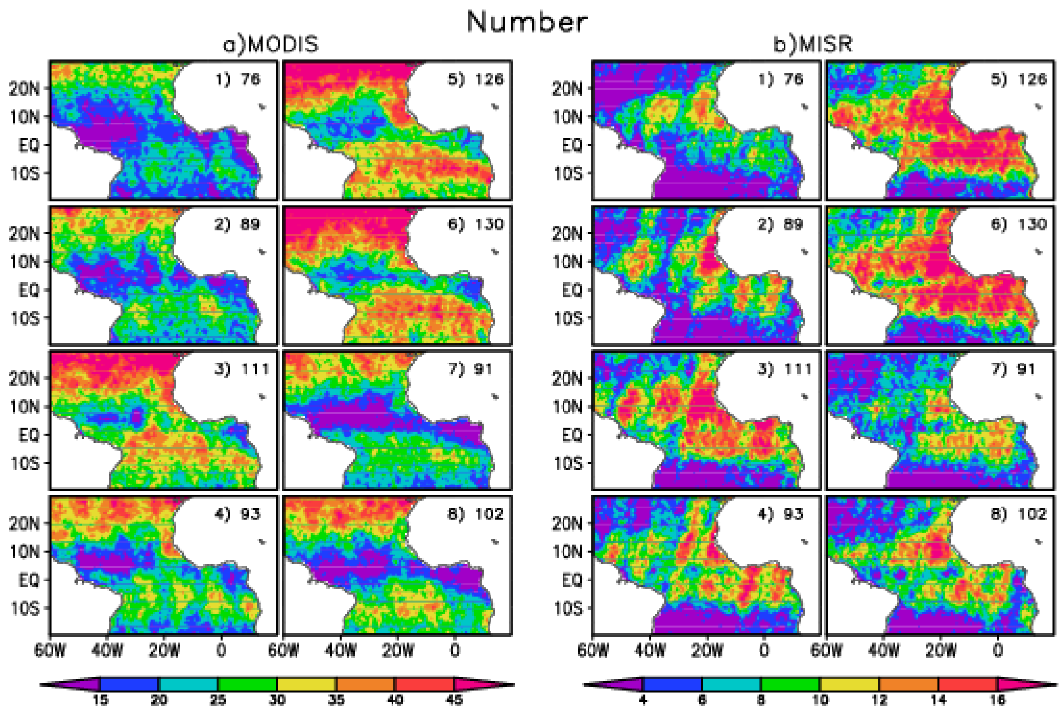

Figure 8: The number of strong MJO events used for MJO composite for each phase of the MJO cycle for a) MODIS and b) MISR during the 2002–2009 boreal winters. The total number of strong MJO events during this period is indicated at the right upper corner of each panel.

826

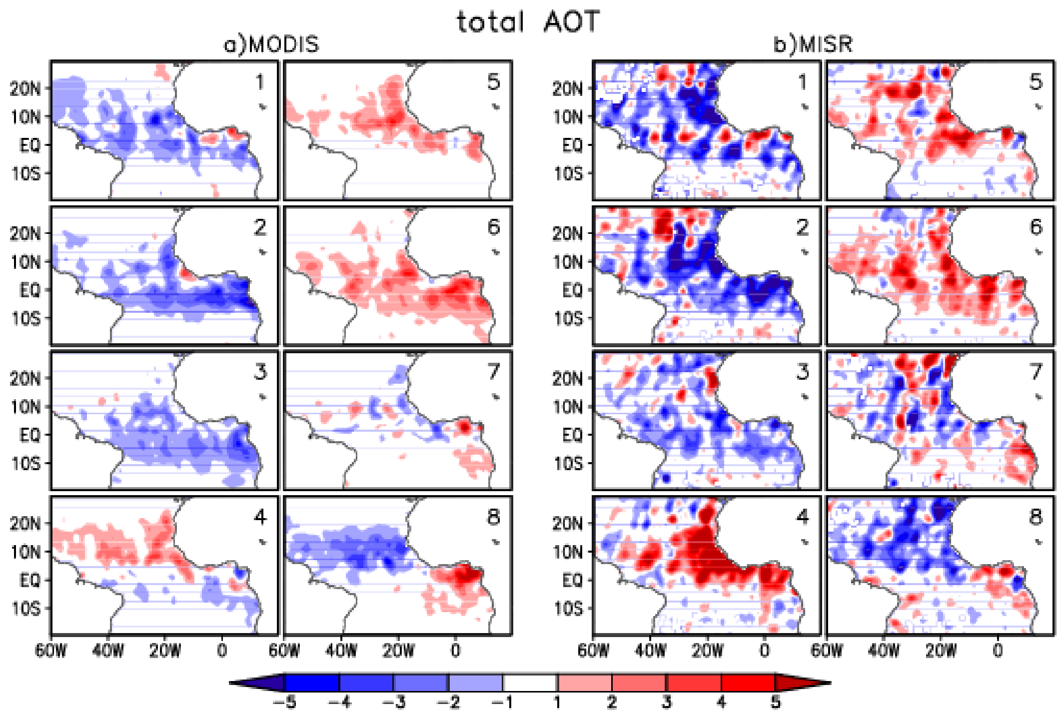

827 **Figure 9**: MJO composite maps of total τ anomalies (multiplied by 100) for a) MODIS

828 and b) MISR over the tropical Atlantic Ocean. 9-point spatial smoothing is applied.

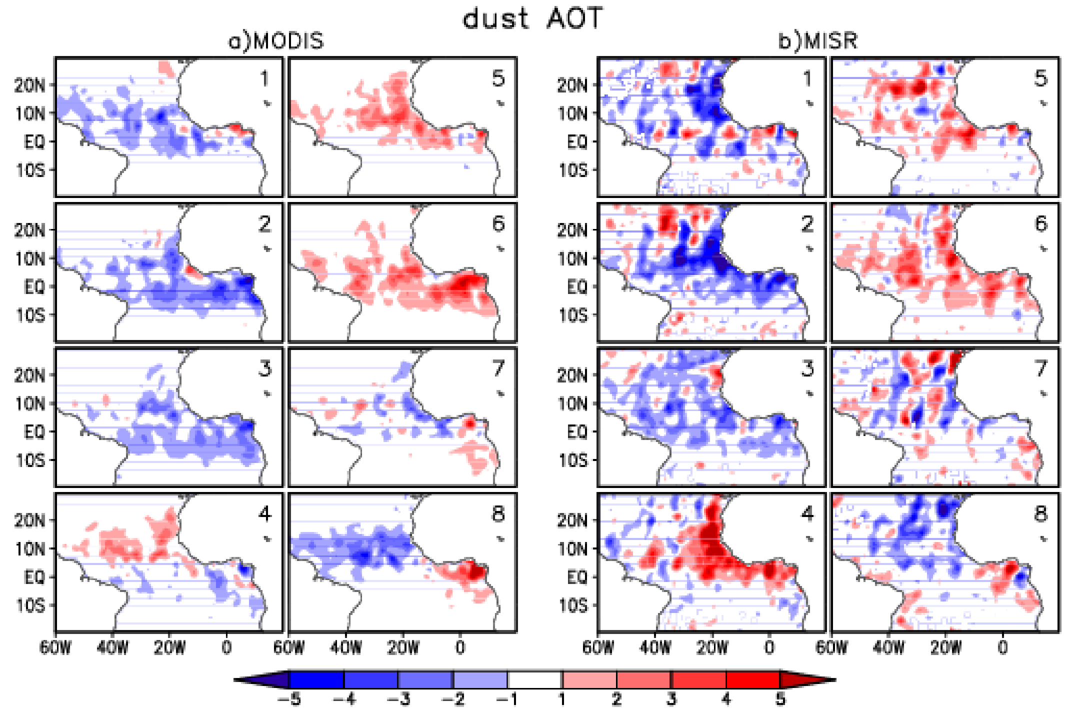

Figure 10: Same as Figure 9, but for τ_{dust}.

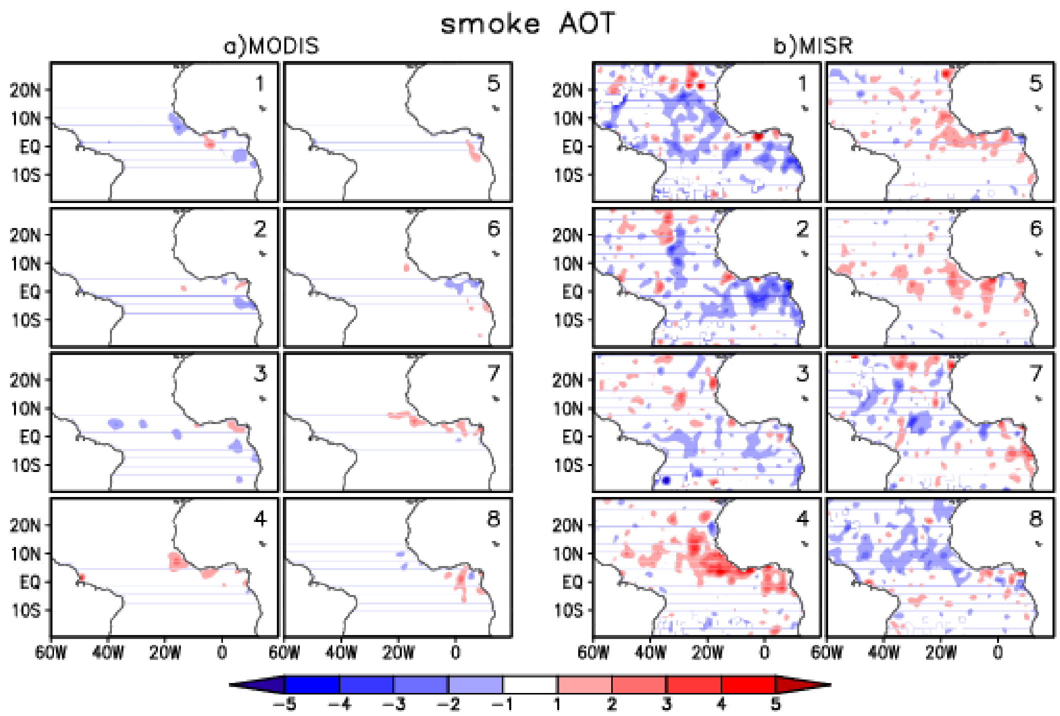

Figure 11: Same as Figure 9, but for τ_{smoke}.

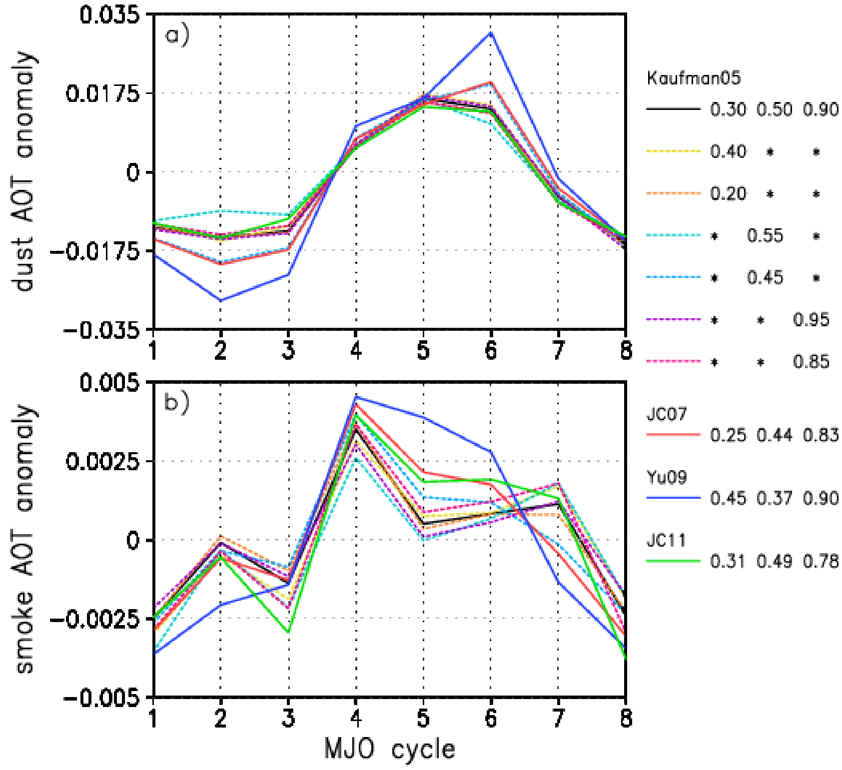

Figure 12: The composite MJO cycle of MODIS a) τ_{dust} and b) τ_{smoke} anomalies averaged over 30 W–15 W, EQ–15 N for the control case (black) and 9 sensitivity test cases (color) with f_{mar}, f_{dust}, and f_{smoke} of each case indicated in the legend.